

# INFLUENCE OF INFLOW STATES OF DYNAMIC WAKE MODEL ON TRIM, ROTOR LOADS AND CONTROL RESPONSE OF A HELICOPTER IN FORWARD FLIGHT

**Lokeswara Rao. V<sup>1</sup>**

<sup>1</sup>Manager, Ph.D. Candidate  
Rotary Wing Research and  
Design Center,  
Hindustan Aeronautics Limited,  
Bangalore-37, India  
[dyna.rwrdc@hal-india.com](mailto:dyna.rwrdc@hal-india.com)

**M. Rohin Kumar<sup>2</sup>**

<sup>2</sup>Senior project engineer  
Department of  
Aerospace Engineering,  
Indian Institute of Technology  
Kanpur-208016, India  
[kumar.rohin@gmail.com](mailto:kumar.rohin@gmail.com)

**C. Venkatesan<sup>3</sup>**

<sup>3</sup>HAL Chair Professor  
Department of  
Aerospace Engineering,  
Indian Institute of Technology,  
Kanpur-208016, India  
[cven@iitk.ac.in](mailto:cven@iitk.ac.in)

## Abstract

A crucial step in the design of rotorcraft is the prediction of oscillatory loads produced by the periodic aerodynamic environment of the helicopter rotor. These oscillatory loads cause vibrations in the helicopter. The vibrations normally pervade both the rotor and the airframe and can seriously degrade service life as well as ride qualities. Accurate prediction of helicopter oscillatory / dynamic loads and response requires the development of multidisciplinary comprehensive analysis program which combines structure, aerodynamic and inertial operators. In this study, one such comprehensive analysis model is described. The model includes elastic flap-lag-torsion and axial blade deformations, modified ONERA dynamic stall theory for airloads calculation, and Peters-He dynamic wake theory for inflow computation. In the present study the number of state variables representing the inflow are varied from 3 states to 45 states by increasing the number of harmonics and radial functions, and their effects on helicopter trim, rotor loads and control response are analysed. Results indicate that there is a clear redistribution of inflow with the increase in number of inflow states. In general there is an increase in the inflow from forward to the aft of the rotor disk with the increase in number of states. It is important to note that there is no significant change in the trim variables with the increase in number of inflow states. However with the inclusion of higher harmonic inflow states, the harmonic content increase in sectional loads and blade root loads. Higher inflow states are seen to affect helicopter control response to longitudinal input at high speeds.

## NOMENCLATURE

### Symbols

$a$	torque offset or lift curve slope	$\{\bar{F}\}$	generalised aerodynamic load vector
$a_d, a_l, a_m$	parameter used in dynamic stall model	$H_n^m$	parameter used in dynamic wake model
$b$	semi blade chord	$[\bar{K}]$	stiffness matrix in modal space
$c$	chord	$K_n^m$	parameter used in dynamic wake model
$[\bar{C}]$	damping matrix in modal space	$L$	lift on airfoil
$C_{dL}, C_{mL}, C_{zL}$	linear static drag co-efficient extrapolated to the stall region	$[\tilde{L}^c], [\tilde{L}^s]$	influence coefficients matrices
$\Delta C_d, \Delta C_m, \Delta C_z$	difference between extrapolated linear static coefficients and measured static coefficients	$l$	length of the blade
$D$	drag on airfoil	$l_e$	length of finite element
$d, d_m$	parameters used in dynamic stall model	$m$	mass per unit length of blade
$e_1, e_2$	root offset	$M$	moment on airfoil, total number of harmonics
$\hat{e}_x, \hat{e}_y, \hat{e}_z$	unit vector along x, y, z axes	$[\bar{M}]$	mass matrix in modal space
$E_d, E_m, E_l$	parameters used in dynamic stall model	$m, p$	harmonic number
		$n, j$	polynomial number
		$N$	number of finite elements
		$N_b$	number of blades in main rotor
		$p_f, q_f, r_f$	angular velocity components at c.g of helicopter

$P_j^P(\bar{v})$	legendre polynomial function
$\bar{P}_j^P(\bar{v})$	normalised legendre polynomial function
$r$	radial distance
$\bar{r}$	nondimensional radial coordinate, $r/R$
$r_d, r_m, r_l$	parameters used in dynamic stall model
$R$	main rotor blade radius
$s, s_m$	parameters used in dynamic stall model
$S$	total inflow states
$\tilde{S}$	area per unit span of airfoil
$T$	kinetic energy
$u_f, v_f, w_f$	translational velocity components at c.g of helicopter
$t$	time
$U$	strain energy
$u_1, v_1, w_1, \phi_1$	
$u_2, v_2, w_2, \phi_2$	
$v'_1, w'_1, v'_2, w'_2$	
$u_{12}, \phi_{12}$	element nodal degrees of freedom
$V$	oncoming velocity
$V_T, V_R$	velocity terms used in inflow model
$W$	weight of the helicopter
$W_e$	external work due to non conservative forces
$X, l$	parameters used in dyanmic wake model
$X_k$	coordinate along k <sup>th</sup> blade axis
$x, y, z$	coordinates of point in $\hat{e}_x - \hat{e}_y - \hat{e}_z$
$\alpha_j^P, \beta_j^P$	induced flow coefficients
$\tilde{\alpha}, \tilde{k}$	parameters used in dyanmic stall model
$\beta_d$	blade predroop angle
$\beta_p$	blade precone angle
$\beta_s$	blade presweep angle
$\Gamma_1$	aerodynamic state in unstalled region in lift equation
$\Gamma_2$	aerodynamic state in stalled region in lift equation
$\Gamma_{d2}$	aerodynamic state in stalled region in drag equation
$\Gamma_{m2}$	aerodynamic state in stalled region in moment equation
$\Lambda_a$	tip anhedral angle
$\Lambda_s$	tip sweep angle
$\lambda$	total inflow ratio
$\lambda_i$	induced inflow ratio
$\mu$	advance ratio
$\rho$	density of air
$\rho_j^P$	normalised factor in dynamic wake

$\sigma, \sigma_d, \sigma_m, \bar{\sigma}_m$	parameters used in dynamic stall model
$\tau_n^{mc}, \tau_n^{ms}$	coefficients of pressure expansion
$\phi_j^P$	radial shape function
$\chi$	wake skew angle
$\psi$	azimuthal angle
$\psi_k$	azimuthal angle of k <sup>th</sup> blade
$\Omega$	rotational frequency of the rotor
$\{\eta_j\}$	vector of modal degree of freedom
$\theta_0$	collective pitch angle
$\theta_{1c}, \theta_{1s}$	cyclic pitch angles
$\theta_{0T}$	tail rotor collective pitch angle
$\Theta$	fuselage attitude in pitch
$\Phi$	fuselage attitude in roll

### Subscripts

$\delta(\ )$	variation ( )
$(\ )_{1k}$	quantities in rotating 1k system
$(\ )_{2k}$	quantities in rotating 2k system
$(\ )_{3k}$	quantities in rotating 3k system
$(\ )_{4k}$	quantities in rotating 4k system
$(\ )_e$	quantities in rotating e system
$(\dot{\ })$	derivative w.r.t. time
$(n)!!$	double factorial of n

## 1. INTRODUCTION

Helicopters operate in a very complex dynamic and aerodynamic environment. The unsteady aerodynamic environment and dynamic response of the flexible rotor blades produces a high oscillatory and vibratory blade loads. These oscillatory loads of the helicopter rotor are a major factor in rotor design as they cause vibrations in the helicopter. The vibrations normally pervade both the rotor and the airframe and can seriously degrade service life as well as ride qualities. Accurate prediction of helicopter vibratory loads is a key thrust area with in the field of rotor aeromechanics since it involves a highly nonlinear aeroelastic response problem.

Formulation of the complete aeroelastic equations of motion requires interaction of structural, aerodynamic, and inertia terms. The structural dynamic modeling of the coupled bending, torsion, and axial deformation of helicopter rotor blades has already reached a high level of maturity making use of finite element or multibody techniques [1 - 6]. The aerodynamic modeling of the rotor involves the determination of the inflow at the rotor disk and then

the calculation of the airloads on the rotor blades. Methods for calculating the inflow range in complexity from the uniform inflow model to dynamic inflow/wake [7-12] and free-wake models. Because of the difficulties in predicting stall and its effect using the theoretical unsteady aerodynamics tools, researchers depend on empirical or semi empirical models. Several mathematical models that attempt to predict the effect of dynamic stall are available in literature. The ONERA dynamic stall model [13] is a relatively simple and efficient model, which can be easily incorporated in any aeroelastic analysis.

In recent years, several aeroelastic studies were undertaken by combining different aerodynamic models representing the rotor wake effects and the unsteady aerodynamics loads on a typical section of a rotor blade [14-16]. The complexity of helicopter simulation requires the development of a comprehensive analysis program that integrates all the disciplines involved in the study. Several comprehensive analysis codes were developed both in academia and in the helicopter industry. A brief history of comprehensive analysis has been given in [17-19].

Laxman et al. [20] formulated a computational aeroelastic model by integrating the structural model, the dynamic wake model, and the dynamic stall model for the prediction of trim and response of a helicopter rotor system in steady, level, forward flight. The rotor-fuselage coupling was not taken into account. Rohin et al. [21] extended the study of Laxman to manoeuvring flight condition using dynamic wake and dynamic stall aerodynamic models and by including rotor-fuselage coupling. In references [20-21] the Peters-He dynamic wake model for inflow with three states were used for prediction of trim and control response analysis of helicopter for forward flight and steady level turns. The three state Peters-He model is equivalent to Pitt-Peters dynamic inflow model and doesn't exploit its full potential. The objectives of this paper are (i) Present the development of a comprehensive analysis for helicopter with the inclusion of higher / multiple inflow states for Peters-He dynamic wake model, (ii) Study the effects of multiple inflow states on helicopter trim angles, blade root loads and control response of the vehicle in level forward flight.

The following sections of this paper describe the model formulation and solution procedure. Some results are compared with flight test data for validation.

## 2. AEROELASTIC MODEL FORMULATION

The complete aeroelastic model requires the

formulation equation of motion, representing the structural model of the rotor blade, aerodynamic model for the evaluation of the sectional loads on the blade and rotor inflow model.

### 2.1. Elastic rotor blade model

The structural portion of the aeroelastic model is based on the elastic blade equation of motion. The elastic rotor blades are idealized as long, slender beams undergoing moderate deformations in axial, bending and torsional modes. The coupling effects between axial, bending and torsional deformations are designated using non-linear strain displacement model. Transverse shear, out of plane warping characteristics of the blades are included in this formulation. The nonlinear kinematics of deformation is based on the mechanics of curved rods [22]. The blade structural formulation in this paper is identical to the model developed in [23]. Radial non uniformities of mass, stiffness, twist, etc., chordwise offset of mass center and shear center, blade sweep, precone, pretwist, root offset, and torque offset are included. The rotor blade with most general geometry is shown in Fig. 1. The coupled flap-lag-torsion-axial equations of motion of the hingeless rotor blade have been derived using Hamilton's principle.

$$(1) \quad \int_{t_1}^{t_2} (\delta U - \delta T - \delta W_e) dt = 0$$

Where  $U$ ,  $T$ ,  $W_e$  represent the strain energy, kinetic energy, and virtual work of external loads, respectively  $\delta$  represents a variation.

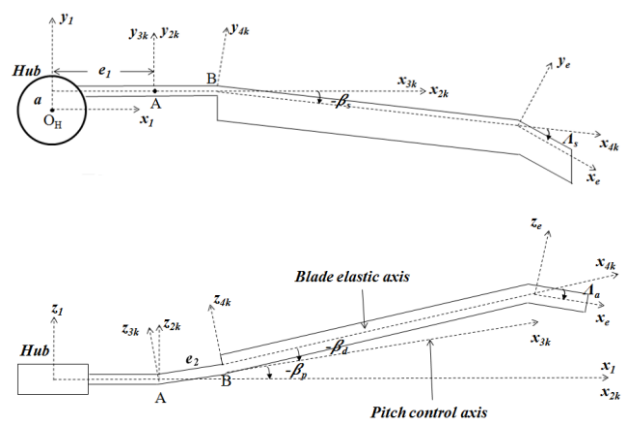


Figure 1: Rotor blade with a most general geometry

The governing partial differential equations obtained using Hamilton's principle is solved using finite element method in time and space. The blade is discretised into sub-regions using beam type finite

elements as shown in Fig. 2, and each element has 14 degrees of freedom as shown in Fig. 3. They corresponding to 4 flap, 4 lag, 3 torsional and 3 axial degrees of freedom. A cubic Hermite polynomial used as an interpolation function for bending deflections and quadratic Lagrangian polynomial is used for torsional rotation and axial deflection. A linear structural dynamic problem is solved in finite element domain to obtain the rotating mode shapes and frequencies of the rotor blade. The blade response is evaluated in the modal space with four flap modes, two lag modes, one torsion and one axial mode in rotating system.

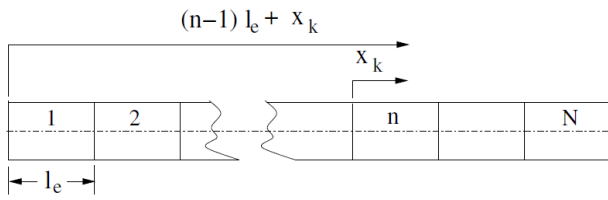


Figure 2: Finite element model of a blade

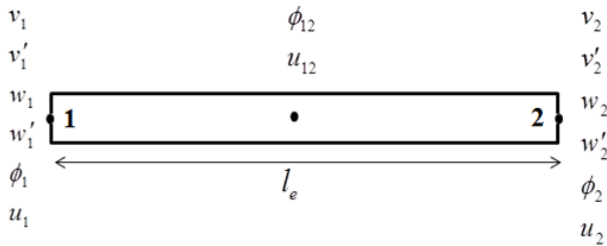


Figure 3: Element nodal degree of freedom

The equation of motion in modal space can be written as

$$(2) \quad [\bar{M}]\{\ddot{\eta}\} + [\bar{C}]\{\dot{\eta}\} + [\bar{K}]\{\eta\} = \{\bar{F}\}$$

Where  $\{\bar{F}\}$  represents the generalized aerodynamic load vector. More details of the equations can be found in [21].

## 2.2. Aerodynamic model

Modeling of rotary-wing aerodynamics requires consideration of two important aspects, namely, estimation of sectional aerodynamic loads on the rotor blade and evaluation of inflow through rotor disk. Fig. 4 shows several models of varying sophistication available for both aspects of rotary-wing aerodynamics. A systematic study was done [20-21] to analyse the influence of different aerodynamic models on helicopter trim and aeroelastic response of rotor blades. It was concluded that the combination of Peters-He dynamic wake model for inflow and *modified*

ONERA model for sectional loads shows good correlation with flight tests. For the present study which is an extension of work in [21], shall focus mainly on the Peters-He dynamic wake model with multiple inflow states and *modified* ONERA dynamic stall model. Both these models are formulated as a set of differential equations and very suitable for aeroelastic equations.

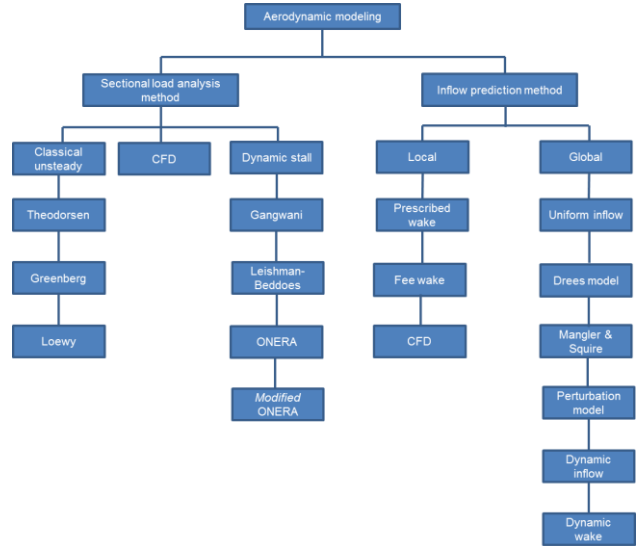


Figure 4: Aerodynamic models

### 2.2.1. Sectional aerodynamic loads (modified ONERA model)

The modified ONERA dynamic stall model provides time variation of lift, moment, and drag on an oscillating aerofoil. The stall model assumes that the lift, moment, and drag are acting at the quarter chord point. The unsteady lift acting normal to the resultant velocity is given as

$$(3) \quad L = \frac{1}{2} \rho \tilde{s} [sb\dot{W}_0 + \tilde{k}b\dot{W}_1 + V\Gamma_1 + V\Gamma_2]$$

Where  $\Gamma_1$ ,  $\Gamma_2$  are evaluated using the following equations.

$$(4) \quad \begin{aligned} \ddot{\Gamma}_1 + B_2 \left(\frac{V}{b}\right) \dot{\Gamma}_1 + B_3 \left(\frac{V}{b}\right)^2 \Gamma_1 &= A_3 \left(\frac{V}{b}\right)^2 \frac{\partial C_{zL}}{\partial \theta} W_0 \\ &+ A_3 \sigma \left(\frac{V}{b}\right)^2 W_1 + A_2 \left(\frac{V}{b}\right) \frac{\partial C_{zL}}{\partial \theta} \dot{W}_0 + A_2 \sigma \left(\frac{V}{b}\right) \dot{W} \\ &+ A_1 \frac{\partial C_{zL}}{\partial \theta} \ddot{W}_0 + A_2 \sigma \ddot{W}_1 \end{aligned}$$

$$(5) \quad \ddot{\Gamma}_2 + a_l \left( \frac{V}{b} \right) \dot{\Gamma}_2 + r_l \left( \frac{V}{b} \right)^2 \Gamma_2 = - \left[ r_l \left( \frac{V}{b} \right)^2 V \Delta C_z|_{w_0/V} + E_l \left( \frac{V}{b} \right) \dot{W}_0 \right]$$

The unsteady moment on the aerofoil is given as

$$(6) \quad M = \frac{1}{2} \rho \tilde{S} 2b \left[ V^2 C_{mL}|_{w_0/V} + (\bar{\sigma}_m + d_m) b \dot{W}_0 \right] + \sigma_m V W_1 + s_m b \dot{W}_1 + V \Gamma_{m2}$$

Where  $\Gamma_{m2}$  is evaluated using the following equation

$$(7) \quad \ddot{\Gamma}_{m2} + a_m \left( \frac{V}{b} \right) \dot{\Gamma}_{m2} + r_m \left( \frac{V}{b} \right)^2 \Gamma_{m2} = - \left[ r_m \left( \frac{V}{b} \right)^2 V \Delta C_m|_{W_0/V} + E_m \left( \frac{V}{b} \right) \dot{W}_0 \right]$$

The unsteady drag acting along the resultant velocity is given as

$$(8) \quad D = \frac{1}{2} \rho \tilde{S} \left[ V^2 C_{dL}|_{W_0/V} + \sigma_d b \dot{W}_0 + V \Gamma_{d2} \right]$$

Where  $\Gamma_{d2}$  is evaluated using the following equation.

$$(9) \quad \ddot{\Gamma}_{d2} + a_d \left( \frac{V}{b} \right) \dot{\Gamma}_{d2} + r_d \left( \frac{V}{b} \right)^2 \Gamma_{d2} = - \left[ r_d \left( \frac{V}{b} \right)^2 V \Delta C_d|_{W_0/V} + E_d \left( \frac{V}{b} \right) \dot{W}_0 \right]$$

Where  $\Delta C_z|_{w_0/V}$ ,  $\Delta C_m|_{w_0/V}$ ,  $\Delta C_d|_{w_0/V}$  are the difference between the linear static aerodynamic coefficients extrapolated to the stalled region to the actual static aerodynamic coefficient of lift, moment and drag respectively, measured at an effective angle of attack,  $W_0/V$ . The quantities  $\Delta C_{mL}|_{W_0/V}$ ,  $\Delta C_{dL}|_{W_0/V}$  are the static moment and drag coefficients in linear regime measured at an effective angle of attack,  $W_0/V$ . The various constants defined in Eqs. (3)– (9) are given in [11].

### 2.2.2. Inflow model (Peters-He dynamics wake)

Although the Pitt-Peters dynamic inflow model [11, 24] has significantly improved the inflow modeling, it still has some limitations because the dynamic inflow model is developed only upto two harmonics and for each harmonic, only one radial shape function is

used for induced inflow. Therefore its application is limited to a means of accounting for rotor wake dynamics of low frequency. Furthermore it is only a low order approximation. For investigation of rotorcraft vibration, higher harmonic control, aeroelasticity dynamic response and aeroelastic tailoring, there is a need for a more sophisticated and efficient inflow model that can deal with higher harmonic, and higher radial modes of induced flow distribution. This limitation is overcome in generalised dynamic wake theory developed by Peters and He [8-9].

The generalised dynamic wake theory developed by Peters and He is based on acceleration potential method for an actuator disc. This model allows for arbitrary number of inflow states. The inflow expression includes variation in both azimuthal and radial directions. The induced flow distribution can be represented as an infinite series in terms of a harmonic variation in azimuth and arbitrary radial distribution functions which is expressed as

$$(10) \quad \lambda(\bar{r}, \psi, t) = \sum_{p=0}^{\infty} \sum_{j=p+1, p+3, \dots}^{\infty} \phi_j^p(\bar{r}) [\alpha_j^p(t) \cos(p\psi) + \beta_j^p(t) \sin(p\psi)]$$

Where the radial function  $\phi_j^p(\bar{r}) = \bar{P}_j^p(\bar{v}) / v$

The term  $\bar{P}_j^p(\bar{v}) / v$  represents Legendre polynomials with the nondimensional radial parameter is given by

$$\bar{v} = \sqrt{1 - \bar{r}^2}$$

The radial function  $\phi_j^p(\bar{r})$  can be expanded as

$$(11) \quad \phi_j^p(\bar{r}) = \frac{1}{\sqrt{(2j+1)H_j^p}} \sum_{q=p, p+2, \dots, (q-p)!!(q+p)!!(j-q-1)!!}^{j-1} \bar{r}^q \frac{(-1)^{(q-p)/2} (j+q)!!}{(q-p)!!(q+p)!!(j-q-1)!!}$$

$$(12) \quad H_j^p = \frac{(j+p-1)!!(j-p-1)!!}{(j+p)!!(j-p)!!}$$

In Eq.10, the parameters  $\alpha_j^p(t)$ , and  $\beta_j^p(t)$  associated with harmonics represent the inflow states.

The inflow states are evaluated by solving governing equations which are a set of first order differential equations

$$(13) \quad [M] \begin{Bmatrix} \vdots \\ \alpha_j^p \\ \vdots \end{Bmatrix} + [V_c] [\tilde{L}^c]^{-1} \begin{Bmatrix} \vdots \\ \alpha_j^p \\ \vdots \end{Bmatrix} = \frac{1}{2} \begin{Bmatrix} \vdots \\ mc \\ \vdots \end{Bmatrix}$$

$$(14) [M] \begin{Bmatrix} \vdots \\ \beta_j^p \\ \vdots \end{Bmatrix} + [V_s] [\tilde{L}^s]^{-1} \begin{Bmatrix} \vdots \\ \beta_j^p \\ \vdots \end{Bmatrix} = \frac{1}{2} \begin{Bmatrix} \vdots \\ \tau_n^{ms} \\ \vdots \end{Bmatrix}$$

In the above Eqs.13 and 14, the subscripts  $j, n$  corresponds to radial functions, superscripts  $p, m$  represent the harmonics and superscripts  $c, s$  represent cosine and sine components. The linear operator  $[M]$  associated with acceleration part of the induced flow, hence it is called as the apparent mass matrix, and it is a diagonal matrix.  $[\tilde{L}^c]$ , and

$[\tilde{L}^s]$  denote the cosine and sine influence coefficient matrices respectively.  $[V_c], [V_s]$  represent velocity

matrices.  $\tau_n^{mc}, \tau_n^{ms}$  represents the cosine and sine components of the aerodynamic loads acting on the rotor system. Closed form expressions for various quantities are given below. The apparent mass matrix is given as

$$(15) [M] = \begin{bmatrix} \ddots & & & \\ & K_n^m & & \\ & & \ddots & \\ & & & \ddots \end{bmatrix}$$

Where  $K_n^m = \frac{2}{\pi} H_n^m$

The influence co-efficient matrices are given by

$$(16) [\tilde{L}^c] = [\tilde{L}_{jn}^{pm}]^c \text{ and } [\tilde{L}^s] = [\tilde{L}_{jn}^{pm}]^s$$

$$(17) [\tilde{L}_{jn}^{0m}]^c = X^m [\Gamma_{jn}^{0m}]$$

$$(18) [\tilde{L}_{jn}^{pm}]^c = \left[ X^{|m-p|} + (-1)^l X^{|m+p|} \right] [\Gamma_{jn}^{pm}]$$

$$(19) [\tilde{L}_{jn}^{pm}]^s = \left[ X^{|m-p|} - (-1)^l X^{|m+p|} \right] [\Gamma_{jn}^{pm}]$$

Where  $l = \min(p, m)$ ,  $X = \tan\left(\frac{\chi}{2}\right)$  and  $\chi$  is the wake skew

angle. The term  $\Gamma_{jn}^{pm}$  is defined as

for even  $(p+m)$

$$(20) \Gamma_{jn}^{pm} = \frac{(-1)^{\frac{n+j-2p}{2}} 2\sqrt{(2n+1)(2j+1)}}{\sqrt{H_n^m H_j^p} (j+n)(j+n+2) [(j-n)^2 - 1]}$$

for odd  $(p+m)$  and  $j = n \pm 1$

$$(21) \Gamma_{jn}^{pm} = \frac{\pi \operatorname{sgn}(p-m)}{\sqrt{H_n^m H_j^p} \sqrt{(2n+1)(2j+1)}}$$

for odd  $(p+m)$  and  $j \neq n \pm 1$

$$(22) \Gamma_{jn}^{pm} = 0$$

$$(23) H_n^m = \frac{(n+m-1)!!(n-m-1)!!}{(n+m)!!(n-m)!!}$$

Velocity matrix is given as follows

$$(24) [V_c] = \begin{bmatrix} V_T & & & \\ & V_R & & \\ & & \ddots & \\ & & & V_R \end{bmatrix}$$

$$(25) [V_s] = \begin{bmatrix} V_R & & & \\ & V_R & & \\ & & \ddots & \\ & & & V_R \end{bmatrix}$$

$$(26) V_T = \sqrt{\mu^2 + \lambda^2}$$

$$(27) V_R = \frac{\mu^2 + \lambda(\lambda + \lambda_i)}{\sqrt{\mu^2 + \lambda^2}}$$

The cosine and sine components of the aerodynamic loads acting on the rotor system are defined in terms of blade lift weighted with radial polynomial function  $\phi_n^m(\bar{r})$ . The expressions for the rotor loads are defined as

$$(28) \tau_n^{0c} = \frac{1}{2\pi} \sum_{k=1}^{N_b} \left[ \frac{1}{\rho \Omega^2 R^3} \int_0^1 \frac{L_k}{\Omega^2 R^3} \phi_n^0(\bar{r}) d(\bar{r}) \right]$$

$$(29) \tau_n^{mc} = \frac{1}{\pi} \sum_{k=1}^{N_b} \left[ \frac{1}{\rho \Omega^2 R^3} \int_0^1 \frac{L_k}{\Omega^2 R^3} \phi_n^m(\bar{r}) d(\bar{r}) \right] \cos(m\psi_k)$$

$$(30) \tau_n^{ms} = \frac{1}{\pi} \sum_{k=1}^{N_b} \left[ \frac{1}{\rho \Omega^2 R^3} \int_0^1 \frac{L_k}{\Omega^2 R^3} \phi_n^m(\bar{r}) d(\bar{r}) \right] \sin(m\psi_k)$$

The equations in Eq.10 are written for an infinite number of azimuthal harmonics and radial shape functions. For practical purpose, the number of harmonics and shape functions used in the modeling of the pressure distribution and induced velocity field must be finite. The induced velocity field may be assumed as

$$(31) \lambda(\bar{r}, \psi, t) = \sum_{p=0}^N \sum_{j=p+1, p+3, \dots}^{2S_p + p - 1} \phi_j^p(\bar{r}) [\alpha_j^p(t) \cos(p\psi) + \beta_j^p(t) \sin(p\psi)]$$

Where  $N$  is the highest harmonic in the azimuthal direction and  $S_p$  is the number of radial shape functions for the  $p^{th}$  harmonic. The choice of inflow states is based on the relationships in Table 1.

Table 1 shows the number of radial shape functions for each harmonic ( $p$ ) in order to have radial terms up to a given power of  $\bar{r}$ . For example, for terms up to  $\bar{r}^4$ , the  $p = 0$  harmonic would have three radial terms; the  $p = 1$  and  $p = 2$  sine and cosine harmonics would have 2 terms each; and the  $p = 3$  and  $p = 4$  sine and cosine harmonics would have one term each. Thus, a total of 15 terms (or state variables) would be used. If more number of polynomials are desired without increasing the total number of harmonics, a row corresponding to a larger power of  $\bar{r}$  has to be chosen. For example, for  $p = 4$  and  $\bar{r}^8$ , this would be  $5 + 2(4 + 4 + 3 + 3) = 33$  total states, denoted as  $S=33$  states. Whereas, if the total number of inflow states is calculated using all harmonic values for  $\bar{r}^8$ , the value would be 45, which is given in the last column of the Table 1.

Table 1: Number of shape functions per harmonic

Highest Power of $\bar{r}$	Harmonic number, $p$								Total Inflow States	
	0	1	2	3	4	5	6	7		8
0	1									1
1	1	1								3
2	2	1	1							6
3	2	2	1	1						10
4	3	2	2	1	1					15
5	3	3	2	2	1	1				21
6	4	3	3	2	2	1	1			28
7	4	4	3	3	2	2	1	1		36
8	5	4	4	3	3	2	2	1	1	45

### 3. NUMERICAL SOLUTION

Rotary-wing aeroelasticity brings together the structural and aerodynamic models described in the previous section. In addition to these models, the helicopter flight dynamic equations have to be added to perform the trim analysis and rotor aeroelastic response. Hence comprehensive analysis of helicopter is a coupled rotor-fuselage analysis. An analytical model representing the coupled rotor/fuselage aeroelastic trim and control response

analysis for a conventional helicopter with hingeless rotor blades has been formulated. The solution technique aims to obtain the helicopter trim and blade response simultaneously by solving in time domain the three sets of equations namely, (i) equations representing elastic deformation of the rotor blade (Eq. (2)), (ii) equations representing inflow through the rotor disc (Eq. (10)), and (iii) sectional aerodynamic loads representing lift, drag and moment acting on the rotor blade (Eqs. (3) - (8)).

A description of the number of variables for the dynamic stall model and dynamic wake model with varied inflow states from 3 to 45 is given in the following: The aerodynamic loads on the rotor blade were calculated at 15 equidistant radial stations. It may be noted that there are four state variables for lift, two state variables each for drag and pitching moment. Therefore, the total number of state variables representing the sectional aerodynamics for one blade is 120 (15 radial stations x 8 state variables per station). The rotor blade structural model is represented by eight modes consisting of four flap modes, two lag modes, one torsion mode and one axial mode. Hence, the total number of state variables representing the structural modes per blade is 16. Depending on the number of inflow states and the number of blades, the total numbers of state variables of the problem vary. For three inflow states, and for a four bladed rotor system, the total number of state variables is 547. They are 480 ( $=4*120$ ) aerodynamic state variables, + 64 ( $=4*16$ ) structural state variables + 3 inflow state variables. On the other hand, for forty-five inflow states, the total number of state variables becomes 589 ( $=4*120+4*16+45$ ).

In the present study, a four bladed system with proper spacing in the azimuthal angle is considered for the analysis. And also the number of state variables representing the inflow is varied from 3 states to 45 states depending on the number of harmonics and radial functions considered for the dynamic wake model. By solving the response of all the blades simultaneously, one can identify the difference in the response of the blades as they go around the azimuth. Since, the response and loads of all the blades are solved at every instant of time, the time varying hub loads and the time varying inflow can be captured. Aerodynamics loads acting on fuselage, horizontal tail, vertical tail and tail rotor are included along with the main rotor loads for the estimation of helicopter trim and response characteristics.

### 3.1. Trim procedure

The flow chart of the procedure used for the coupled rotor/fuselage trim analysis of a helicopter for level forward flight is shown in Fig. 5. A propulsive trim procedure was adopted to obtain the main rotor control angles, tail rotor collective angle and fuselage attitudes.

The algorithm has two iterative loops; the inner loop comprises three sets of differential equations representing the blade sectional loads, rotor inflow and blade response. The differential equations are solved using Runge-Kutta integration scheme. The outer loop solves the trim problem which is a set of nonlinear algebraic equations [21]. These nonlinear algebraic trim equations are solved using Newton-Raphson method. Thus the inner loop deals with the rotor blade aeroelastic response while the outer loop handles the vehicle as a whole. The program outputs the inflow over the rotor, hub loads, blade response, blade sectional loads, blade shear and bending moments, rotor pilot inputs and vehicle attitudes.

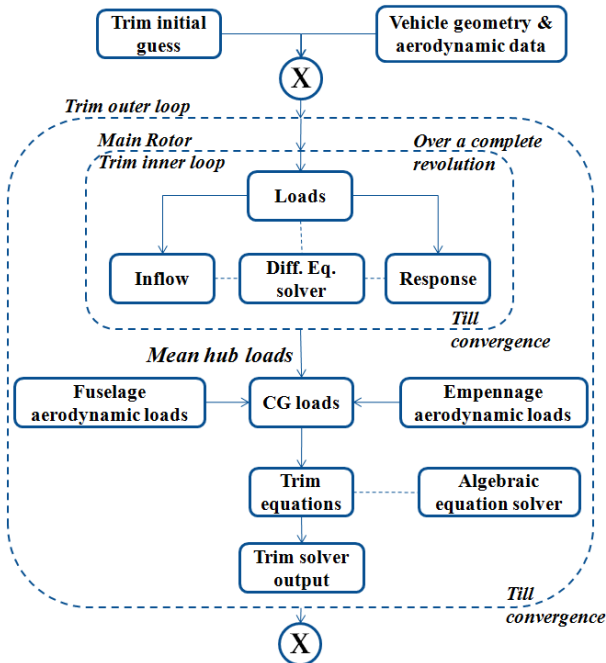


Figure 5: Helicopter trim and rotor response algorithm

### 3.2. Control Response procedure

Figure 6 shows the flow chart of the procedure used for determining the response of the helicopter to pilot control inputs. The control response procedure starts with a perturbation in any one or combination of pilot controls when the vehicle is in trim condition.

Like in the trim procedure, even here there are two loops. However, unlike in the trim procedure, there is no iteration involved in both the loops. After the perturbation in the pilot controls, the rotor equations are solved for loads, inflow and response per time step increment. The rotor hub loads along with the fuselage and empennage are transformed to the center of gravity to satisfy the vehicle equation of motion. The control response is determined by integrating the full set of nonlinear equations of motion of the vehicle with respect to time. More details of these equations can be found in [21]. The resulting solution is the set of vehicle states (translational velocities, angular velocities and attitudes) at the end of that time step. The whole process is repeated for each subsequent time step to evaluate the time evolution of the rotor blade and vehicle response. The algorithms shown in Fig. 5 and 6 were implemented as c++ program using the open source GSL [25] as the math library.

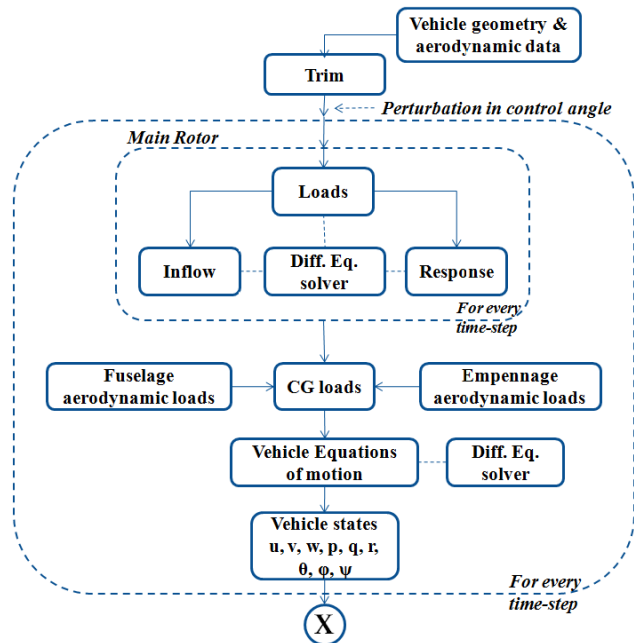


Figure 6: Helicopter control response algorithm

## 4. RESULTS AND DISCUSSION

Using the solution technique described in the previous section, results pertaining to trim angles, blade sectional loads, root loads, inflow and helicopter control response characteristics in level forward flight with respect to the total inflow states,  $S$  are obtained and plotted. For the sake of conciseness, only the results pertaining to inflow states of  $S = 3, 10, 15, 21$  and  $45$  are discussed. The vehicle and blade data used in the present study are given in Table 2. The helicopter modeled is a conventional type single main and tail rotor.

Main rotor blade is modeled as a hingeless rotor blade, and rotor system consists of four blades.

Table 2: Vehicle and blade properties

Parameter	Symbol	Value	Units
Air density	$\rho$	0.954	kg/m <sup>3</sup>
Main Rotor			
Number of blades		4	
Non-dimensional blade chord	$c/R$	0.0757	
Solidity ratio	$\sigma$	0.09646	
Weight coefficient	$C_w$	0.00734	
Pre-Twist		-12	degrees
Lift curve slope	$cl_\alpha$	5.73	
Profile drag coefficient cd0 0.01			
Lock number	$\gamma$	6.4	
Torque offset		0.0015	
Predroop		2.5	degree
Modal frequencies of rotor blade			
Lag		0.71, 5.30	
Flap		1.09, 2.88,	
		5.01, 7.57	
Torsion		4.37	
Axial		33.36	
Vehicle			
Equivalent flat plate area		0.0131	
Parasite drag coefficient		1	

The variation of control angles and fuselage attitudes in pitch and roll with the forward speeds for the inflow states of  $S = 3, 10, 15, 21$  and  $45$  are shown in Fig. 7. The analytical results have been correlated with the flight data [26]. It can be observed that the estimated trim values match reasonably well with the flight data. It is also noted that there are no significant changes in trim variables with the variation of inflow states.

Figure 8 shows azimuthal variation of the sectional aerodynamic lift (8a), drag (8b) and moment (8c) at  $0.95R$  with forward speeds for various inflow states. It is seen that the harmonic content increase with the inclusion of higher harmonic inflow states. There is a marked dip in the minimum pitching moment (8c) in the second quadrant at higher inflow states. It is also observed that the sectional loads converge beyond 10 inflow states.

The integration of the sectional forces or moments outboard of any section provides the shear force and bending moment at that section. The variation of the blade root shear forces and bending moments with azimuth for various inflow states with the advance ratio of  $0.3$  are shown in Fig. 9. Just as for the sectional loads, the root shear and bending moments show increase in harmonic content with

increase in number of inflow states. The loads are observed to converge for states higher than 10.

Figure 10 shows the contour plots of the inflow variation on the rotor disc for higher harmonics inflow states at an advance ratio of  $0.3$ . The inflow distribution significantly changes over the rotor disc for higher inflow states. It is seen that there is an increase in the inflow from forward to the aft of the rotor disc.

Figures 11-14 show the control response plots for step input of  $1$  deg., in lateral and longitudinal cyclic for hover and  $\mu = 0.25$  for various inflow states. For analysis, the response during the initial couple of seconds is more important. From Figs. 11 and 12, it is seen that there is not much influence of the number of inflow states on the roll control response in hover. But the pitch response shows a deviation for higher inflow states. From Fig 13, it is seen that at high speeds ( $\mu = 0.25$ ), there is not much effect of the number of inflow states on the pitch and roll rates for lateral cyclic step input. It is only for the longitudinal cyclic step input at high speed (Fig 14), the pitch and roll rates are seen to vary drastically with change in inflow states. This aspect needs to be analysed further.

## 5. CONCLUDING REMARKS

In this paper, a systematic study was undertaken to analyse the effects of multiple inflow states of dynamic wake model on trim, rotor loads and control response of helicopter in forward flight. The important observations of this study can be summarized as follows.

- (i) The results of the present study shows that there is a clear redistribution of inflow pattern with the increase in number of inflow states. In general there is an increase in the inflow from forward to the aft of the rotor disk.
- (ii) The trim variables for the forward flight are observed to be in good agreement with the flight test data. It is important to note that there is no significant change in the trim variables with the increase in number of inflow states.
- (iii) Blade loads are seen to have higher harmonic content with increase in the number of inflow states.
- (iv) The tip sectional loads and blade root loads curves are seen to converge beyond 10 inflow states. For the 4 bladed rotor considered in this study, 15 inflow states (4 harmonics) seems to be sufficient to capture the inflow effects.
- (v) Higher inflow states are seen to affect response to longitudinal input at high speeds.

**ACKNOWLEDGMENTS**

The first author wishes to acknowledge the financial support provided by RWR&DC management of Hindustan Aeronautics Limited, India, for conducting this research study at IIT-Kanpur.

**REFERENCES**

- [1] Houbolt, J.C., and Brooks, G.W., "Differential Equations of Motion for Combined Flapwise Bending, Chordwise Bending and Torsion of Twisted Nonuniform Rotor Blades," *NACA Report 1346*, 1958.
- [2] Hodges, D.H., and Dowell, E.H., "Nonlinear Equations of Motion for the Elastic Bending and Torsion of Twisted Non-uniform Rotor Blades," *NASA TN D-7818*, 1974.
- [3] Kaza, K.R., and Kvaternik, R.G., "Nonlinear Aeroelastic Equations for Combined Flapwise Bending, Chordwise Bending, Torsion and Extension of Twisted Nonuniform Rotor Blades in Forward Flight," *NASA TM-74059*, 1977.
- [4] Bauchau, O.A., and Kang, N.K., "A Multibody Formulation for Helicopter Structural Dynamic Analysis," *Journal of the American Helicopter Society*, April 1993, pp. 3-14.
- [5] Kim, K.C., and Chopra, I., "Aeroelastic Analysis of Swept, Anhedral, and Tapered Tip Rotor Blades," *Journal of the American Helicopter Society*, Vol. 37, No. 1, 1992, pp. 15-30.
- [6] Yuan, K.A., Friedmann, P., and Venkatesan, C., "A New Aeroelastic Model for Composite Rotor Blades with Straight and Swept Tips," *AIAA Paper No. 92-2259, Proceedings of 33rd AIAA/ASME/ASCE/AHS/ASC Structures, Structural Dynamics and Materials Conference*, Dallas, TX, April 1992, pp. 1371-1390.
- [7] Johnson, W., *Helicopter Theory*, Princeton University Press, Princeton, NJ, 1980.
- [8] He, C.J., "Development and Application of a Generalized Dynamic Wake Theory for Lifting Rotors," *Ph.D. Thesis*, Georgia Institute of Technology, July 1989.
- [9] Peters, D.A., Boyd, D.D., and He, C.J., "Finite-State Induced-Flow Model for Rotors in Hover and Forward Flight," *Journal of the American Helicopter Society*, Vol. 34, No. 4, 1989, pp. 5-17.
- [10] Peters, D.A., and He, C.J., "Correlation of Measured Induced Velocities with a Finite-State Wake Model," *Journal of the American Helicopter Society*, Vol. 36, No. 3, 1991, pp. 59-70.
- [11] Pitt, D.M. and Peters, D.A., "Theoretical prediction of Dynamic Inflow Derivatives," *Vertica*, Vol. 5, No. 1 (March 1981), pp. 21-34
- [12] Friedman, P. P. and Venkatesan, C., "Finite State Modeling of Unsteady Aerodynamics and its Applications to a Rotor Dynamics Problem," Eleventh European Rotorcraft Forum, London, Paper No. 77 (September 1985).
- [13] Petot, D., "Differential Equation Modeling of Dynamic Stall," *La Recherche Aerospatiale, Paper No. 1989-5*, 1989.
- [14] Peters, D. A., Barwey, D., and Su, A., "An integrated Airloads Inflow Model for Use in Rotor Aeroelasticity and Control Analysis," *Mathematical and Computer modeling*, Vol. 19, (3/4), 1994, pp. 109-123.
- [15] Tang, D., and Dowell, E.H., "Nonlinear Rotor Aeroelastic Analysis with Stall and Advanced Wake Dynamics," *Journal of Aircraft*, Vol. 34, (5), September 1997, pp. 679-687.
- [16] Subramanian, S., Ma, G., Gaonkar, G.H., and Maier, T.H., "Correlation of Several Aerodynamic Models and measurements of Hingeless Rotor Trim and Stability," *Journal of the American Helicopter Society*, Vol. 45, (2), 2000, pp. 106-117.
- [17] Kunz, D.L., "Comprehensive Rotorcraft Analysis : Past, Present and Future," *46th AIAA Structural Dynamics & Materials Conference, AIAA 2005-2244*, Austin, Texas, April 2005.
- [18] Johnson, W., "Rotorcraft Aeromechanics Applications of a Comprehensive Analysis," *Heli Japan 98: AHS International Meeting on Advanced Rotorcraft Technology and Disaster Relief*, Japan, April 1998.
- [19] Johnson, W., "A History of Rotorcraft Comprehensive Analysis," *NASA/TP-2012-216012*, April 2012.
- [20] Laxman, V. and Venkatesan, C., "Influence of Dynamic Stall and Dynamic Wake Effects on Helicopter Trim and Rotor Loads," *Journal of the American Helicopter Society*, Vol. 54, No. 3, July 2009.
- [21] Rohin Kumar, M., Venkatesan, C., "Rotorcraft Aeroelastic Analysis using Dynamic Wake/Dynamic Stall Models and its Validation," *Journal of Aeroelasticity and Structural Dynamics*, Vol. 3, No. 1, 2014.

- [22] G. Wempner. *Mechanics of solids with applications to thin bodies*, Volume 2. Springer, 1981.
- [23] Yuan, K. A., and Friedmann, P. P., "Aeroelasticity and structural optimization of Composite Helicopter Rotor Blades with Swept Tips," *NASA TM-84245*, 1982.
- [24] Peters. D.A. and Ninh HaQuang, "Dynamic Inflow for Practical Application," *Journal of the American Helicopter Society*, Vol. 33, No. 4, Oct 1988.
- [25] GSL – GNU scientific library. <http://www.gnu.org/software/gsl/>.
- [26] Singh, G.D., "Helicopter Flight Dynamics Simulation for Analysis of Trim, Stability and Control," mastersThesis, *Indian Institute of Technology, Kanpur*, India, May 2012.

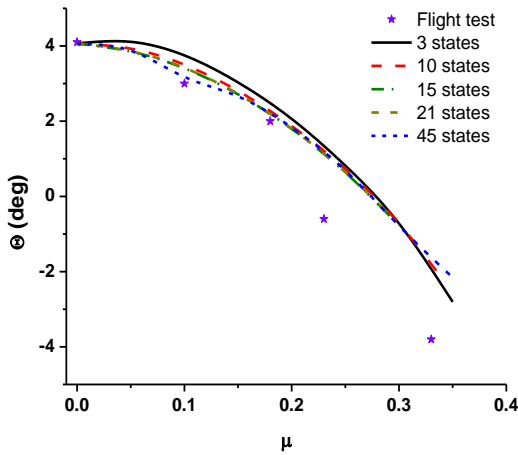


Figure 7a: Vehicle pitch attitude with forward speed.

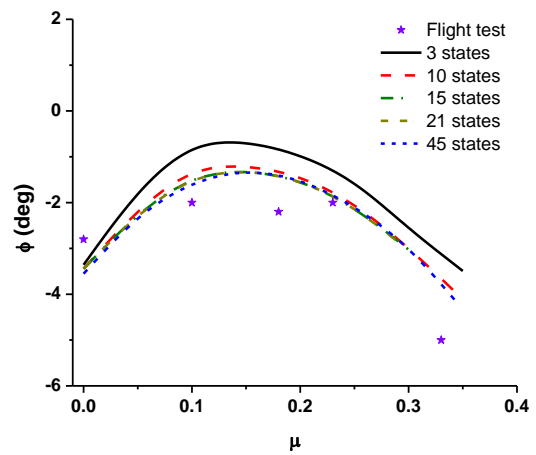


Figure 7b: Vehicle roll attitude with forward speed.

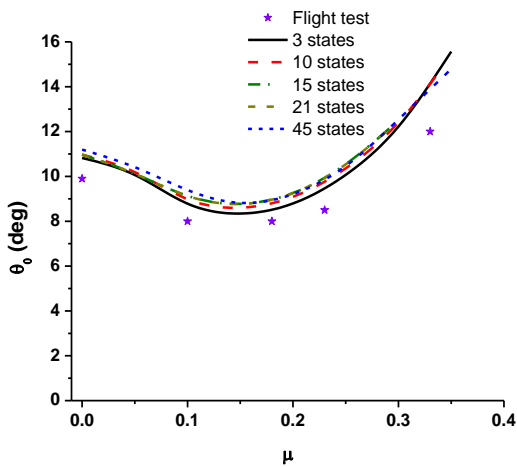


Figure 7c: Main rotor collective variation with forward speed.

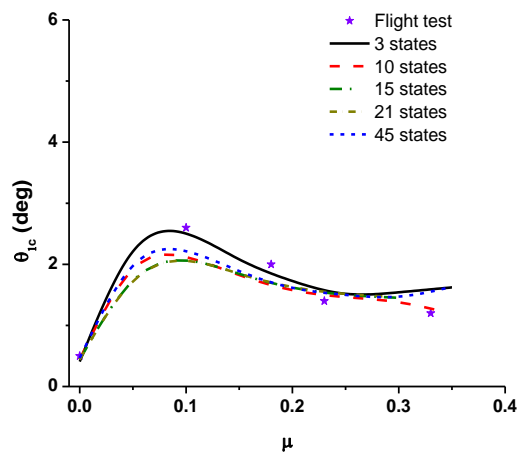


Figure 7d: Lateral cyclic variation with forward speed.

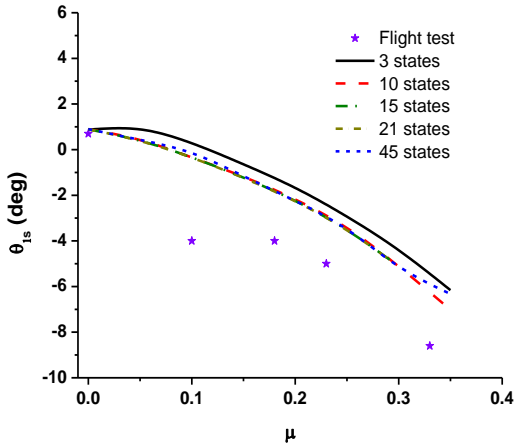


Figure 7e: Longitudinal cyclic variation with forward speed.

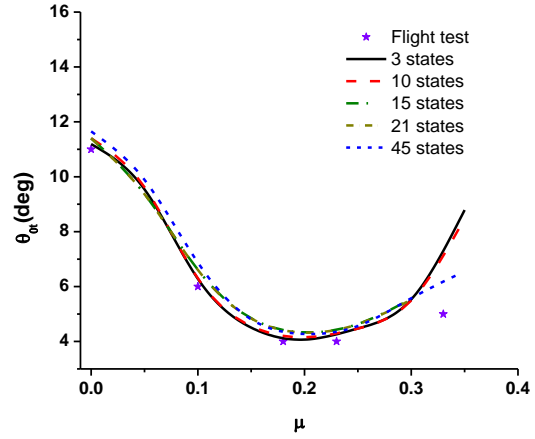


Figure 7f: Tail rotor collective variation with forward speed.

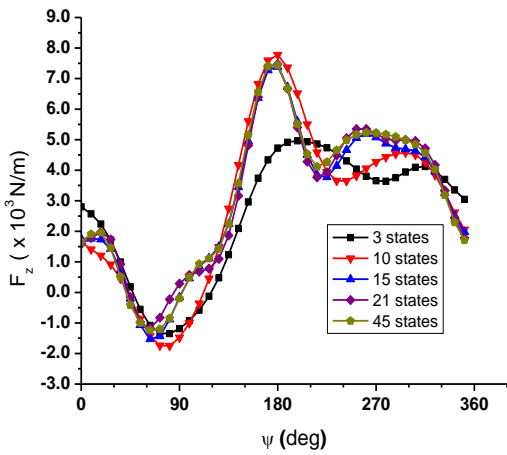


Figure 8a: Sectional aerodynamic lift variation at 0.95R for different inflow states at  $\mu=0.3$ .

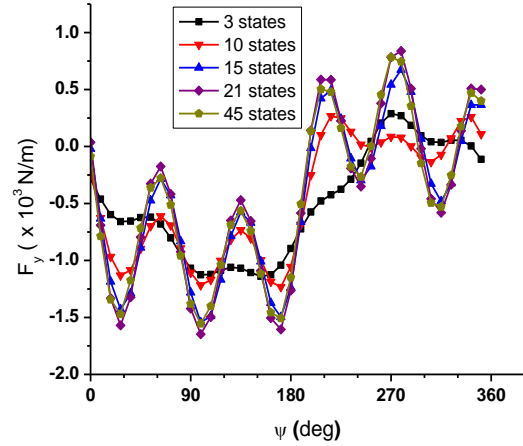


Figure 8b: Sectional aerodynamic drag variation at 0.95R for different inflow states at  $\mu=0.3$ .

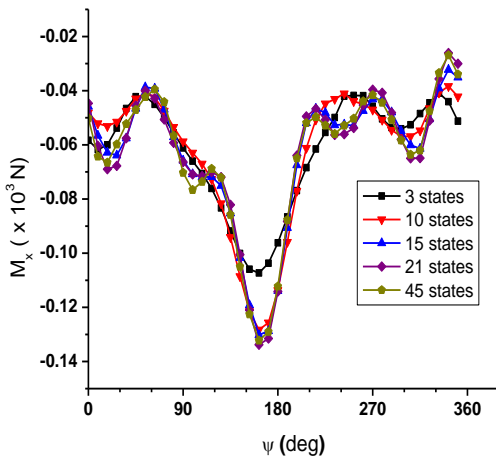


Figure 8c: Sectional aerodynamic pitching moment variation at 0.95R for different inflow states at  $\mu=0.3$ .

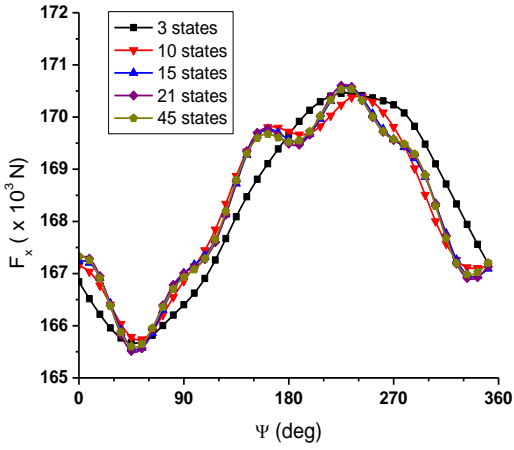


Figure 9a: Blade root axial force for different inflow states at  $\mu=0.3$ .

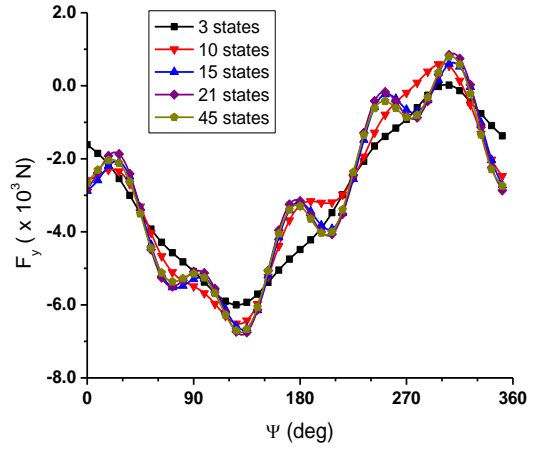


Figure 9b: Blade root lag shear force for different inflow states at  $\mu=0.3$ .

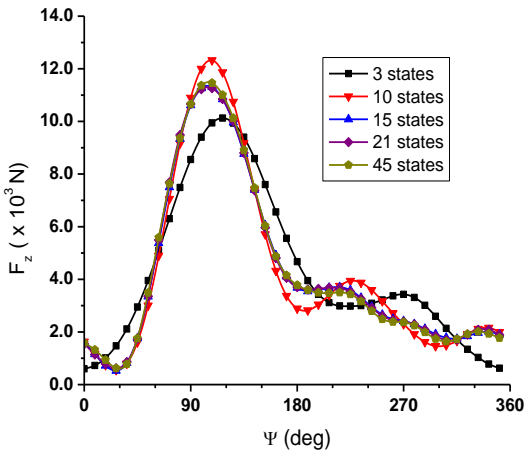


Figure 9c: Blade root vertical shear force for different inflow states at  $\mu=0.3$ .

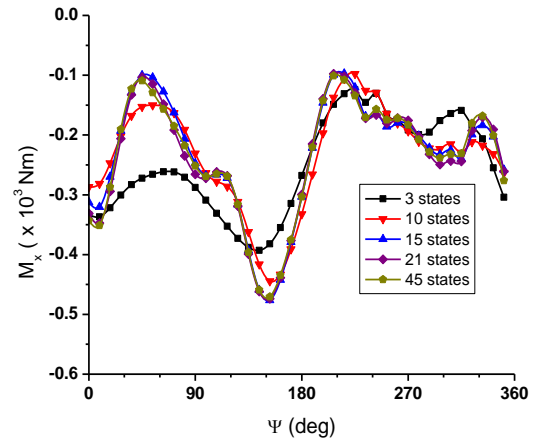


Figure 9d: Blade root pitching moment for different inflow states at  $\mu=0.3$ .

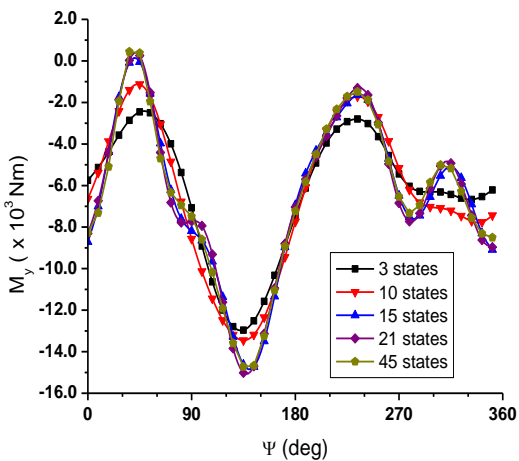


Figure 9e: Blade root flap bending moment for different inflow states at  $\mu=0.3$ .

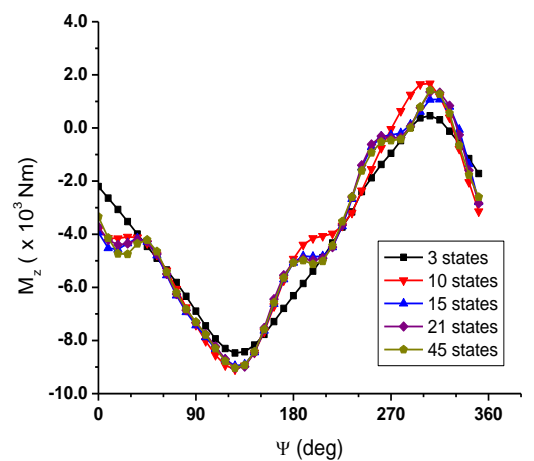


Figure 9f: Blade root lag bending moment for different inflow states at  $\mu=0.3$ .

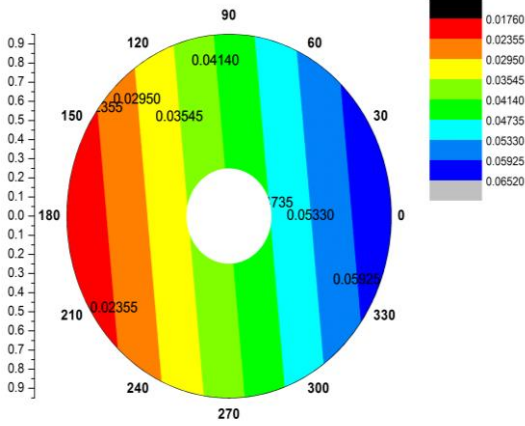


Figure 10a: Rotor induced flow distribution for 3 inflow states at  $\mu=0.3$ .

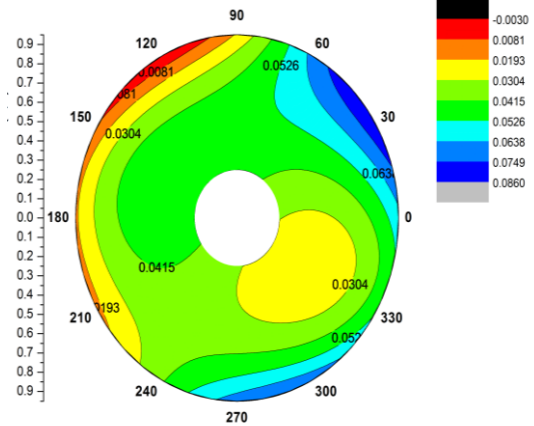


Figure 10b: Rotor induced flow distribution for 10 inflow states at  $\mu=0.3$ .

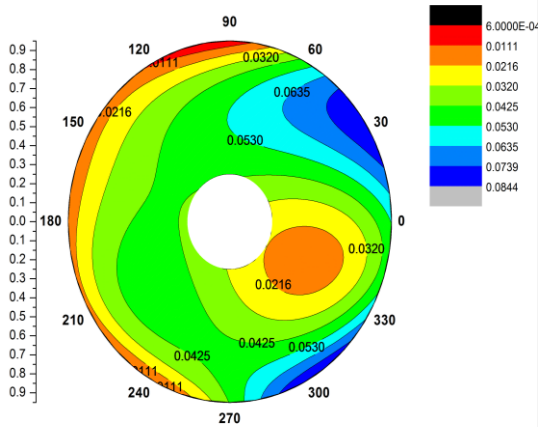


Figure 10c: Rotor induced flow distribution for 15 inflow states at  $\mu=0.3$ .

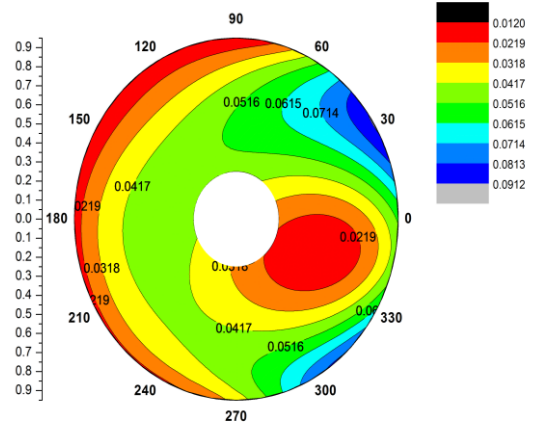


Figure 10d: Rotor induced flow distribution for 21 inflow states at  $\mu=0.3$ .

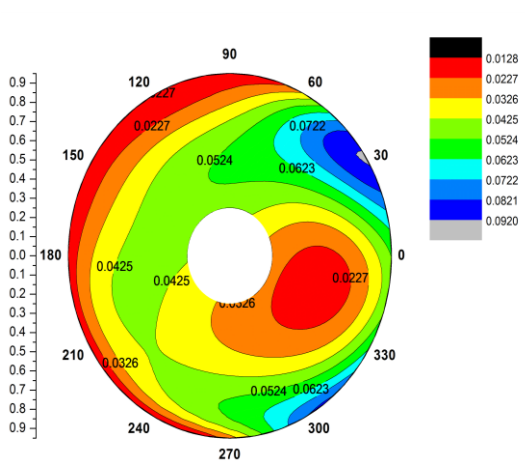


Figure 10e: Rotor induced flow distribution for 36 inflow states at  $\mu=0.3$ .

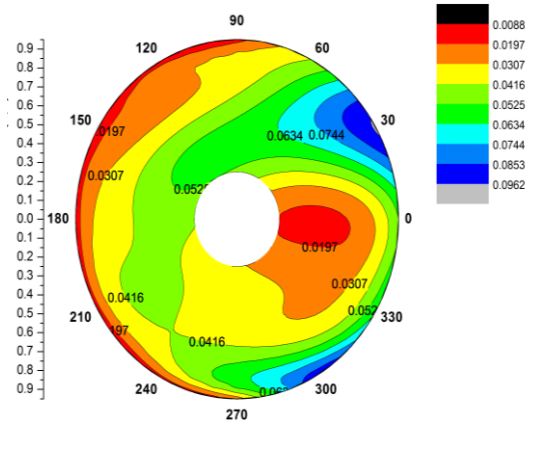


Figure 10f: Rotor induced flow distribution for 45 inflow states at  $\mu=0.3$ .

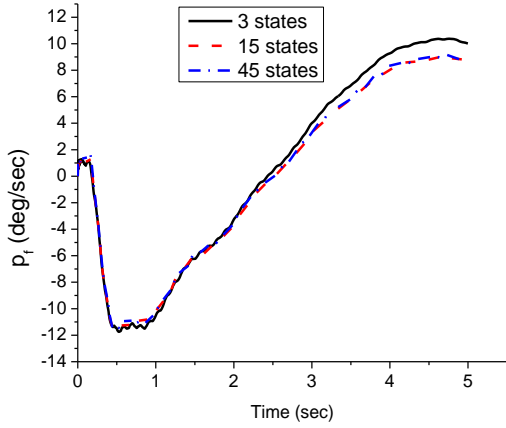


Figure 11(a): Helicopter roll rate response for 1deg. lateral cyclic step input in hover.

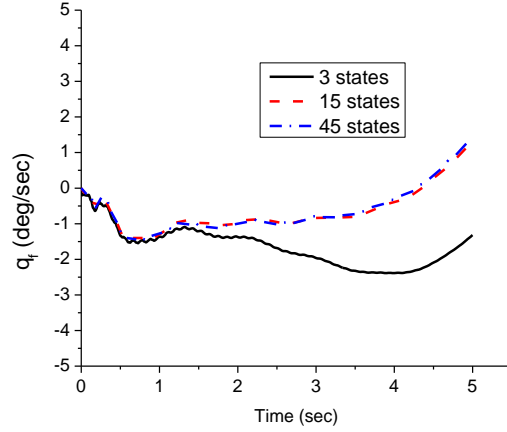


Figure 11(b): Helicopter pitch rate response for 1deg. lateral cyclic step input in hover.

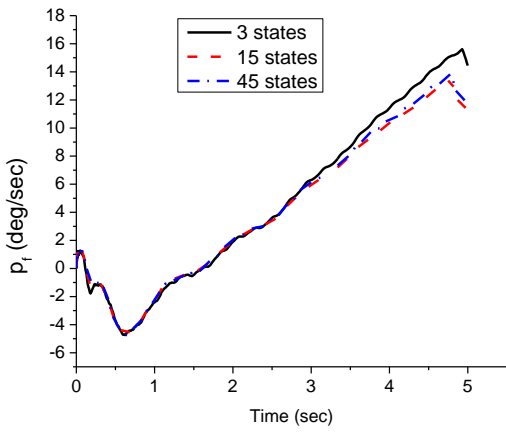


Figure 12(a): Helicopter roll rate response for 1deg. longitudinal cyclic step input in hover.

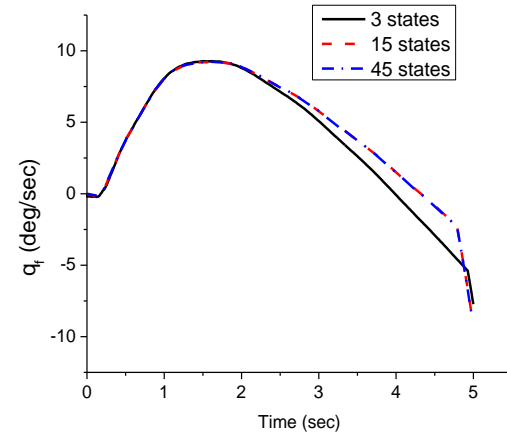


Figure 12(b): Helicopter pitch rate response for 1deg. longitudinal cyclic step input in hover.

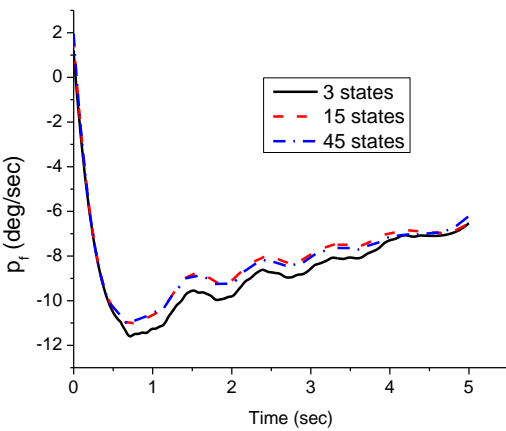


Figure 13(a): Helicopter roll rate response for 1deg. lateral cyclic step input at  $\mu=0.25$ .

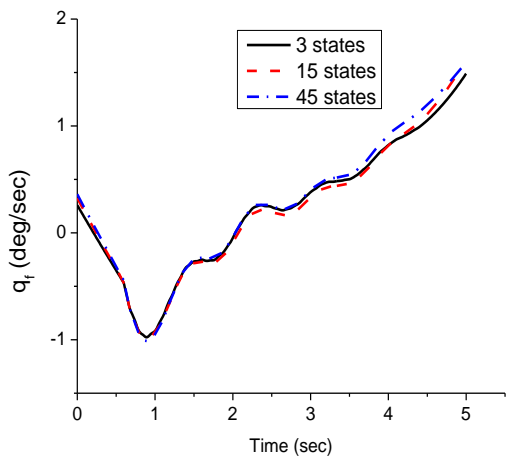


Figure 13(b): Helicopter pitch rate response for 1deg. lateral cyclic step input at  $\mu=0.25$ .

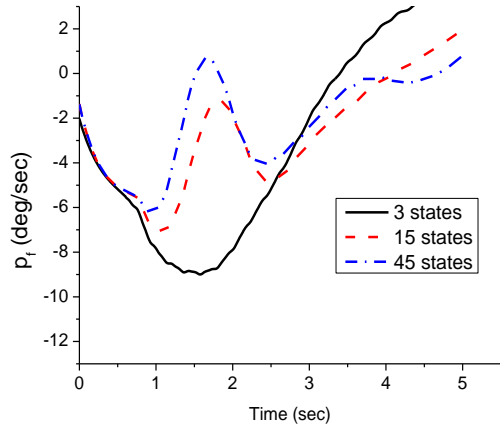


Figure 14(a): Helicopter roll rate response for 1deg. longitudinal cyclic step input at  $\mu=0.25$ .

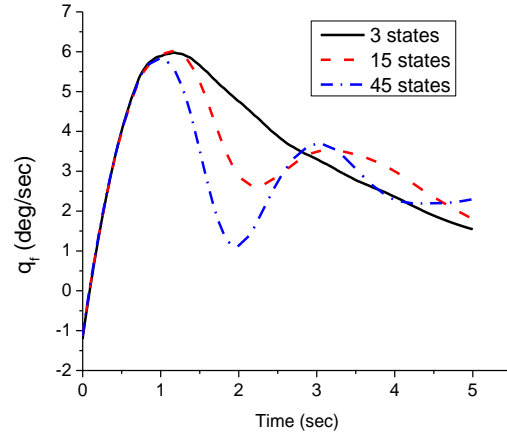


Figure 14(b): Helicopter pitch rate response for 1deg. longitudinal cyclic step input at  $\mu=0.25$ .